

Efficient Degradation-aware Any Image Restoration

Eduard Zamfir¹ Zongwei Wu¹ Nancy Mehta¹
Danda Pani Paudel^{2,3} Yulun Zhang⁴ Radu Timofte¹
¹University of Würzburg ²INSAIT Sofia University
³ETH Zürich ⁴Shanghai Jiao Tong University

Abstract

Reconstructing missing details from degraded low-quality inputs poses a significant challenge. Recent progress in image restoration has demonstrated the efficacy of learning large models capable of addressing various degradations simultaneously. Nonetheless, these approaches introduce considerable computational overhead and complex learning paradigms, limiting their practical utility. In response, we propose *DaAIR*, an efficient All-in-One image restorer employing a Degradation-aware Learner (DaLe) in the low-rank regime to collaboratively mine shared aspects and subtle nuances across diverse degradations, generating a degradation-aware embedding. By dynamically allocating model capacity to input degradations, we realize an efficient restorer integrating holistic and specific learning within a unified model. Furthermore, DaAIR introduces a cost-efficient parameter update mechanism that enhances degradation awareness while maintaining computational efficiency. Extensive comparisons across five image degradations demonstrate that our DaAIR outperforms both state-of-the-art All-in-One models and degradation-specific counterparts, affirming our efficacy and practicality. The source will be publicly made available at <https://eduardzamfir.github.io/daair/>

1 Introduction

Image restoration is a fundamental problem in computer vision, focusing on reconstructing high-quality images from deteriorated observations. Adverse conditions such as noise, haze, or rain significantly impact the practical utility of images in downstream tasks across various domains, including autonomous navigation [43, 4] and augmented reality [13, 39, 8]. Therefore, developing robust image restoration techniques is a critical endeavour. Recent advances in Deep learning-based approaches have shown great achievements in image restoration [55, 41, 20, 58, 26, 3, 53, 5, 23, 7, 10]. However, most of the existing works adopt task-specific learning, targeting a single known degradation at once [57, 26, 53, 5, 3]. This specificity, of one model per task, inherently limits their practicability and hinders their application in diverse degradation settings [50, 51, 32].

To address this limitation, there has been growing interest in All-in-One image restoration models capable of handling various degradations simultaneously. Notable works in this direction [22, 52, 43, 25, 11, 31, 54] employ contrastive [22], meta-learning [54] or visual prompting techniques [31, 44]. Despite their success, these models face two primary limitations. First, these models often overlook the distinct and shared characteristics of each image corruption. Even when certain approaches [25, 54] account for these characteristics, they often rely on external prior information or complex progressive meta-learning, thus failing to harness the inherent potential benefits of self-learning within the network. Second, leveraging auxiliary priors through prompt-learning [31, 44, 23, 10] is a prominent approach. However, their task-specific relevance may be ambiguous, necessitating abundant learnable parameters to capture intricate details, complicating the model interpretability and increasing the overall computational demands.

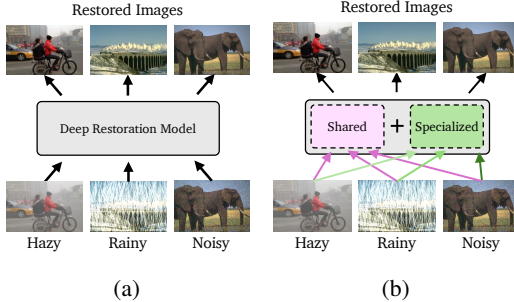


Figure 1: (a) Prior work employ inefficient models and learning for capturing degradation dependencies. (b) We route model capacity to efficiently learn shared and specialized embeddings.

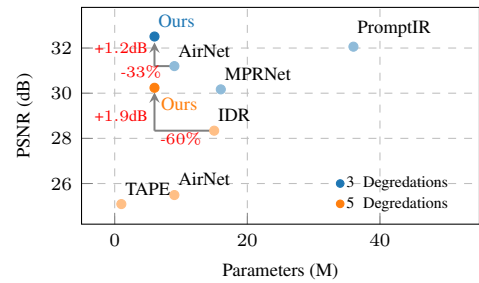


Figure 2: *Model complexity*. Our proposed DaAIR surpasses prior methods, achieving state-of-the-art results in All-in-One image restoration with enhanced efficiency.

Unlike other works, our objective is to recognize degradation-specific representations while emphasizing the commonalities that unify distinct degradations into a shared underlying representation, leveraging the intricacies among different restoration tasks efficiently. For instance, dehazing and denoising have traditionally been considered separate tasks. Haze manifests as a uniform veil that reduces contrast and makes objects appear less distinct, while noise appears as random variations in pixel values, often resembling graininess. Despite their distinct visual effects, these degradations share similar characteristics: both haze and noise are distributed across the entire image and affect similar aspects, such as edges, textures, and contrasts. Thus, learning how to dehaze should also contribute to denoising tasks. Further, we foresee that such associations are also prevalent in various other degradations.

In this paper, we present DaAIR, which provides novel insights for handling multiple degradations concurrently. Specifically, DaAIR employs a dedicated Degradation-aware Learner (DaLe) to learn both the shared and distinct characteristics of each degradation. A novel degradation-aware routing mechanism is further proposed to explicitly associate model capacity with the target degradation, while simultaneously handling agnostic information across degradation types. As illustrated in Fig. 1, such a design assigns specialized and shared expertise to address the nuanced aspects of different degradations, unifying task specificity and task agnosticity within a single model without any sort of complex learning, thus setting us apart from previous approaches. We leverage this unification to optimize collaborative learning by projecting specialized and shared features into a low-rank latent space, emphasizing the most informative aspects of both features.

In addition, to further tackle the efficiency aspect of our model, we propose a novel cost-efficient parameter update by leveraging the accumulated degradation characteristics from the encoder as an additional supervisory signal for the decoding stage. This self-learnable control mechanism enables cross-task semantic mining, while being guided by the shared common embedding, resulting in better restoration quality. We seamlessly incorporate relevant restoration information with negligible computational overhead. This enhances degradation awareness and results in a lightweight, efficient model. Consequently, our design sets a new benchmark for All-in-One image restoration in terms of efficiency and fidelity, as demonstrated in Fig. 2.

Overall, our key contributions are threefold:

- We propose DaAIR which sets a new *state-of-the-art* performance for all-in-one image restoration while being significantly smaller and more efficient compared to prior works.
- We propose a dynamic path uniquely associating degradations to explicit experts while harnessing the shared commonalities between degradations to enrich the degradation-awareness of our model.
- A self-learning mechanism is proposed to utilize the model’s inherent information for improving the image quality, achieving seamless integration of task-relevant cues with minimal computational cost.

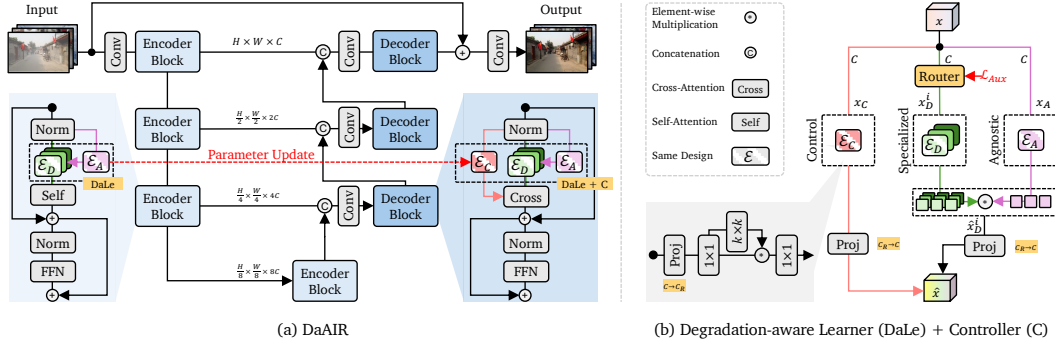


Figure 3: *Architecture overview*. DaAIR reconstructs missing information using an asymmetric encoder-decoder architecture. Each encoder block integrates our proposed Degradation-aware Learner (DaLe) adaptively routing model capacity. Additionally, the decoder blocks are complemented by a controller (C) to enhance overall reconstruction.

2 Related Works

Task Specific Image Restoration. Reconstructing the clean image from its degraded counterpart is a highly ill-posed problem, however, a great body of work have addressed image restoration from a data-driven learning perspective, achieving tremendous results compared to prior hand-crafted methods [55, 41, 20, 58, 24, 53, 45]. Most proposed solutions build on convolutional [55, 41, 58, 3] or Transformer-based architectures [26, 45, 53, 5] addressing single degradation tasks, such as denoising [55, 58, 5], dehazing [36, 35, 47] or deraining [17, 34]. Contrary to CNN-based networks, Transformer offer strong modeling capabilities for capturing global dependencies, which makes them outstanding image restorers [26, 53, 59]. Self-attention’s quadratic complexity w.r.t the image size poses a challenge for resource-constrained applications. Conversely, convolutions provide fast and efficient processing, albeit with limited global processing, and scale more effectively with the input size. In this work, we enhance a Transformer-based architecture [53] by incorporating a dedicated degradation-aware learner for efficiently capturing the shared and distinct context of each degradation.

All-in-One Image Restoration. Research on restoring degraded images has been thorough, but practical implementation is hindered by the need for different models and the challenge of selecting the appropriate one for each task. Images commonly exhibit multiple issues like noise and blur, compounding the difficulty of addressing them individually. An emerging field known as All-in-One image restoration is advancing in low-level computer vision, utilizing a single deep blind restoration model to tackle multiple degradation types simultaneously [52, 43, 4, 18, 31, 54]. The seminal work, AirNet [22], achieves blind All-in-One image restoration by employing contrastive learning to extract degradation representations from corrupted images, which are subsequently utilized to restore the clean image. Next, IDR [54] decomposes image degradations into their underlying physical principles, achieving All-in-One image restoration through a two-stage process based on meta-learning. Prompt-based learning [31, 44, 23] has emerged as a promising research direction. Notably, [31] introduces tunable prompts that encode discriminative information about degradation types, albeit involving a large number of parameters. In contrast, we propose a novel, parameter-efficient approach that meticulously emphasizes the most informative aspects of the relevant features across various degradations.

3 Methodology

In this section, we outline the core principles of our efficient All-in-One image restoration method. As shown in Fig. 3, our pipeline uses a U-shaped architecture [38, 53] with an asymmetric encoder-decoder design. A 3×3 convolution first extracts shallow features from the degraded input, which then pass through 4 levels of encoding and decoding stages. Each level includes several Transformer blocks [53, 31], incorporating our **Degradation-aware Learner** (DaLe) before the attention layer. Unlike previous Transformer-based methods [24, 53, 31], our decoder blocks receive signals from the encoder blocks to help recover the clean output via *controllers*. In each decoder block, we replace

the self-attention layer with cross-attention to facilitate interaction between features computed by the DaLe and the controller blocks. Finally, a global residual connection links the shallow features to the output of the refinement stage, capturing high-frequency details before producing the restored image.

3.1 Degradation-aware Learner

Our objective is to minimize the overall computational complexity while proficiently encapsulating the spatial data crucial for image restoration. We employ efficient experts to modulate the *degradation-specific* and *degradation-agnostic* information within a low-rank framework [15]. Our **Degradation-aware Learner** (DaLe) consists of an agnostic expert (\mathcal{E}_A) and specialized experts (\mathcal{E}_D) for each degradation type. These experts share a common design, projecting into a low-rank space followed by element-wise multiplication of specialized and agnostic features. This approach enhances degradation-dependent representations with contextual cues, exploring inter-dependencies between various degradations like noise or haze. In the decoder, we integrate a controller block within DaLe to guide the restoration process, leveraging accumulated task-specific knowledge from the optimization phase.

Routing. Drawing inspiration from sparse Mixture-of-Experts concepts [40, 37], we integrate linear layers within each DaLe to enable a routing mechanism, associating input features $\mathbf{x} \in \mathbb{R}^{H \times W \times C}$ with their respective specialised degradation experts \mathcal{E}_D . This routing layer \mathcal{R} orchestrates the allocation of same-task training samples to degradation-specific experts \mathcal{E}_D^i , indexed by $i \in 1, \dots, N$, with N representing the total considered degradations, effectively enabling top-1 sparse routing. During training, we employ an auxiliary classification loss \mathcal{L}_{Aux} to infuse task-related knowledge into the routing layers, ensuring they explicitly correlate with the target degradation. Without this, the routers lack a basis for selecting specific experts, leading to randomized routing and thus suboptimal model capacity utilization. The impact of the auxiliary loss on the routing is illustrated in Fig. 5.

Expert design. Each expert contains a projection of their input features into the low-rank approximation $\mathbf{x}_D \in \mathbb{R}^{H \times W \times C_R}$ with $C_R << C$ for emphasizing the most relevant information along the channel dimension, reducing redundancy while allowing for efficient processing in low dimensional space. Next, a large-kernel convolutional block [14], denoted as Conv2Former, captures correlations among pixels within a local neighbourhood, mimicking window-based SA layers [24, 6, 5], while preserving the efficiency benefits of convolutions. Efficient design for the degradation-specific experts, \mathcal{E}_D is more crucial, given the escalating computational demands that arise in direct proportion to the number of experts, which, in turn, is contingent upon the type of degradation under consideration. In light of this, as illustrated in Fig. 3, the normalized input features \mathbf{x} are dispatched to their associated degradation experts via the router \mathcal{R} , partitioning the input batch into groups containing identical degradation training samples. This division allows each expert to specialize within its specific task generating the degradation-specific representation \mathbf{x}_D . Concurrently, the agnostic expert \mathcal{E}_A processes the entire batch, learning a shared representation \mathbf{x}_A across all degradations to complement \mathbf{x}_D with inter-dependencies among different degradations. More concretely, the modulated degradation features $\hat{\mathbf{x}}_D^i$ are obtained as following:

$$\hat{\mathbf{x}}_D^i = \mathcal{E}_D^i(\mathbf{x}_D^i) \odot \mathcal{E}_A(\mathbf{x}_A) \quad (1)$$

$$\text{with } \mathcal{E}_D^i(\mathbf{x}_D^i) = \text{Conv2Former}(\mathbf{W}_{C \rightarrow C_R}^1 \mathbf{x}_D^i) \quad (2)$$

$$\text{and } \mathcal{E}_A(\mathbf{x}_A) = \text{Conv2Former}(\mathbf{W}_{C \rightarrow C_R}^2 \mathbf{x}_A) \quad (3)$$

where linear layers for compressing the channel dimensions are denoted as \mathbf{W} and \odot denotes the Hadamard product. Next, the sub-batches containing $\hat{\mathbf{x}}_D^i$ are merged before a shared linear layer expands the channel dimension back to its original size producing the final degradation-aware features $\hat{\mathbf{x}}$.

3.2 Self-learnable Control

Prompt-based techniques [31, 23, 44] embed task-specific details into trainable parameters that interact with features to enhance them based on degradation types. However, this approach increases model size and computational demands during both training and inference. Moreover, the knowledge encapsulated in the learned prompt parameters remains opaque, complicating efforts to interpret and improve restoration quality. To address this challenge without compromising the accuracy-efficiency

trade-off, we utilize the knowledge stored in the encoder’s agnostic expert to guide parameter updates in the decoder’s controller block. This strategy ensures the optimization process incorporates pertinent information crucial to the restoration task, addressing interpretability concerns linked to prompt-based learning with minimal computational load. The controller block shares the same design as \mathcal{E}_A , allowing to update the learned parameters based on an exponential moving average (EMA) with α as a balancing factor. For guiding the reconstruction process within the decoder branch, we use cross-attention between the controlling features \mathbf{x}_C and the modulated features $\hat{\mathbf{x}}$. The controller features \mathbf{x}_C generate keys, emphasizing pertinent information, while queries and values are derived from modulated features $\hat{\mathbf{x}}$. Cross-attention then refines the restoration process by enabling the model to selectively focus on regions of $\hat{\mathbf{x}}$. In Table 4, we highlight the advantages of our control mechanism. Additionally, the feature visualizations illustrated in Fig. 7 demonstrate the controller’s ability to capture degradation characteristics.

4 Experiments

We conduct experiments by strictly following previous works in general image restoration [31, 54] under two different settings: (i) *All-in-One* and (ii) *Single-task*. In the All-in-One setting, a unified model is trained across multiple degradation types, where we consider *three* and *five* distinct degradations. Within the Single-task setting, separate models are trained for each specific restoration task.

Implementation Details. Our DaAIR framework is end-to-end trainable requiring no multi-stage optimization of any components. The architecture comprises a four-level encoder-decoder structure, with each level containing a different number of transformer blocks, namely [2, 3, 3, 4] from highest to lowest level. The reduction ratio between the embedding and low-rank dimensionality for all experts is 16 and kept constant throughout the network. We follow the training configuration of prior work [31], and train our models for 120 epochs with a batch size of 32 for All-in-One setting and a batch size of 8 for the single task setting. We optimize the L_1 loss using the Adam [19] optimizer ($\beta_1 = 0.9$, $\beta_2 = 0.999$) with an initial learning rate of 2×10^{-4} and cosine decay. During training, we utilize crops of size 128² with horizontal and vertical flips as augmentations.

Datasets. For All-in-One and single-task settings, we follow existing work [22, 31] and include following datasets: For image denoising in single task setting, we combine the BSD400 [1] and WED [27] datasets, adding Gaussian noise at levels $\sigma \in [15, 25, 50]$ to create noisy images. Testing is conducted on the BSD68 [28] and Urban100 [16] datasets. For single-task deraining, we use Rain100L [48]. The single task dehazing task utilises the SOTS [21] dataset. For deblurring and low-light enhancement, we employ the GoPro [30] and the LOL-v1 [46] dataset, respectively. To develop a unified model for all tasks, we merge these datasets in a *three* or *five* degradation setting, and train for 120 epochs and directly evaluate them across different tasks. While, for a single task, our method is trained for 120 epochs on the respective training set.

Table 1: *Comparison to state-of-the-art on three degradations.* PSNR (dB, \uparrow) and SSIM (\uparrow) metrics are reported on the full RGB images. **Best** and **second best** performances are highlighted. Our method sets a new state-of-the-art on average across all benchmarks while being significantly more efficient than prior work. ‘-’ represents unreported results.

Method	Params.	<i>Dehazing</i>		<i>Deraining</i>			<i>Denoising</i>			Average			
		SOTS	Rain100L	BSD68 $_{\sigma=15}$	BSD68 $_{\sigma=25}$	BSD68 $_{\sigma=50}$							
BRDNet [42]	-	23.23	.895	27.42	.895	32.26	.898	29.76	.836	26.34	.693	27.80	.843
LPNet [12]	-	20.84	.828	24.88	.784	26.47	.778	24.77	.748	21.26	.552	23.64	.738
FDGAN [9]	-	24.71	.929	29.89	.933	30.25	.910	28.81	.868	26.43	.776	28.02	.883
DL [11]	2M	26.92	.931	32.62	.931	33.05	.914	30.41	.861	26.90	.740	29.98	.876
MPRNet [52]	16M	25.28	.955	33.57	.954	33.54	.927	30.89	.880	27.56	.779	30.17	.899
AirNet [22]	9M	27.94	.962	34.90	.967	33.92	.933	31.26	.888	28.00	.797	31.20	.910
PromptIR [31]	36M	30.58	.974	36.37	.972	33.98	.933	31.31	.888	28.06	.799	32.06	.913
DaAIR (<i>ours</i>)	6M	32.30	.981	37.10	.978	33.92	.930	31.26	.884	28.00	.792	32.51	.913

Table 2: *Comparison to state-of-the-art on five degradations.* PSNR (dB, \uparrow) and SSIM (\uparrow) metrics are reported on the full RGB images with (*) denoting general image restorers, others are specialized all-in-one approaches. **Best** and **second best** performances are highlighted.

Method	Params.	<i>Dehazing</i>		<i>Deraining</i>		<i>Denoising</i>		<i>Deblurring</i>		<i>Low-Light</i>		Average	
		SOTS	Rain100L	BSD68 $_{\sigma=25}$	GoPro	LOLv1							
NAFNet* [3]	17M	25.23	.939	35.56	.967	31.02	.883	26.53	.808	20.49	.809	27.76	.881
DGUNet* [29]	17M	24.78	.940	36.62	.971	31.10	.883	27.25	.837	21.87	.823	28.32	.891
SwinIR* [24]	1M	21.50	.891	30.78	.923	30.59	.868	24.52	.773	17.81	.723	25.04	.835
Restormer* [53]	26M	24.09	.927	34.81	.962	31.49	.884	27.22	.829	20.41	.806	27.60	.881
DL [11]	2M	20.54	.826	21.96	.762	23.09	.745	19.86	.672	19.83	.712	21.05	.743
Transweather [43]	38M	21.32	.885	29.43	.905	29.00	.841	25.12	.757	21.21	.792	25.22	.836
TAPE [25]	1M	22.16	.861	29.67	.904	30.18	.855	24.47	.763	18.97	.621	25.09	.801
AirNet [22]	9M	21.04	.884	32.98	.951	30.91	.882	24.35	.781	18.18	.735	25.49	.847
IDR [54]	15M	25.24	.943	35.63	.965	31.60	.887	27.87	.846	21.34	.826	28.34	.893
DaAIR (<i>ours</i>)	6M	31.97	.980	36.28	.975	31.07	.878	29.51	.890	22.38	.825	30.24	.910

Table 3: *Comparison to state-of-the-art for single degradations.* PSNR (dB, \uparrow) and SSIM (\uparrow) metrics are reported on the full RGB images. **Best** and **second best** performances are highlighted. Our method excels prior work on dehazing and deraining.

(a) <i>Dehazing</i>		(b) <i>Deraining</i>		(c) <i>Denoising</i>		
Method	SOTS	Method	Rain100L	Method	$\sigma=15$	$\sigma=25$
DehazeNet [2]	22.46 .851	UMR [49]	32.39 .921	IRCNN [55]	33.87 .929	31.18 .882
EPDN [33]	22.57 .863	MSPFN [17]	33.50 .948	FFDNet [56]	33.87 .929	31.21 .882
FDGAN [9]	23.15 .921	LPNet [12]	23.15 .921	BRDNet [42]	34.10 .929	31.43 .885
AirNet [22]	23.18 .900	AirNet [22]	34.90 .977	AirNet [22]	34.14 .936	31.48 .893
PromptIR [31]	31.31 .973	PromptIR [31]	37.04 .979	PromptIR [31]	34.34 .938	31.71 .897
DaAIR (<i>ours</i>)	31.99 .981	DaAIR (<i>ours</i>)	37.78 .982	DaAIR (<i>ours</i>)	34.25 .934	31.61 .891
					28.36 .807	

4.1 Comparison to State-of-the-Art Methods

All-in-One: Three Degradations. We compare our All-in-One restorer with specialized All-in-One restoration methods, including BRDNet [42], LPNet [12], FDGAN [9], DL [11], MPRNet [52], AirNet [22], and PromptIR [31], trained simultaneously on three degradations: dehazing, deraining, and denoising. Our proposed method emerges as the best All-in-One restorer and the most efficient, as demonstrated in Table 1. It consistently outperforms previous works, with an average improvement of 0.45 dB across all benchmarks. Notably, our method achieves state-of-the-art performance on the SOTS and Rain100L benchmarks, surpassing the previously best PromptIR [31] by 1.72 dB and 0.72 dB, respectively, featuring about 83% lesser parameters and 80% lesser GMACS.

All-in-One: Five Degradations. Following recent studies [22, 54], we extend the three degradation settings to include deblurring and low-light image enhancement, validating our method’s effectiveness in a more complex All-in-One setting. As shown in Table 2, our method excels by learning dedicated experts for each degradation while modelling the commonalities between tasks. It outperforms AirNet [22] and IDR [54] by 4.75 dB and 1.9 dB on average across all five benchmarks, using 33% and 60% fewer parameters, respectively. Additionally, we compare our method to general image restoration models trained in the same All-in-One setting. Notably, our method surpasses Restormer [53] and NAFNet [3] on the GoPro test set by 2.29 dB and 2.98 dB, respectively, while being four times and three times smaller in size.

Single-Degradation Results. To assess the efficacy of our proposed framework, we present results in Table 3 wherein individual instances of our method are trained using the single degradation protocol. The single-task variant trained for dehazing consistently outperforms AirNet [22] and PromptIR [31] by 8.81 dB and 0.68 dB, respectively. Similarly, when trained for image deraining, our method surpasses both previous approaches by 3.07 dB and 0.74 dB, respectively, demonstrating

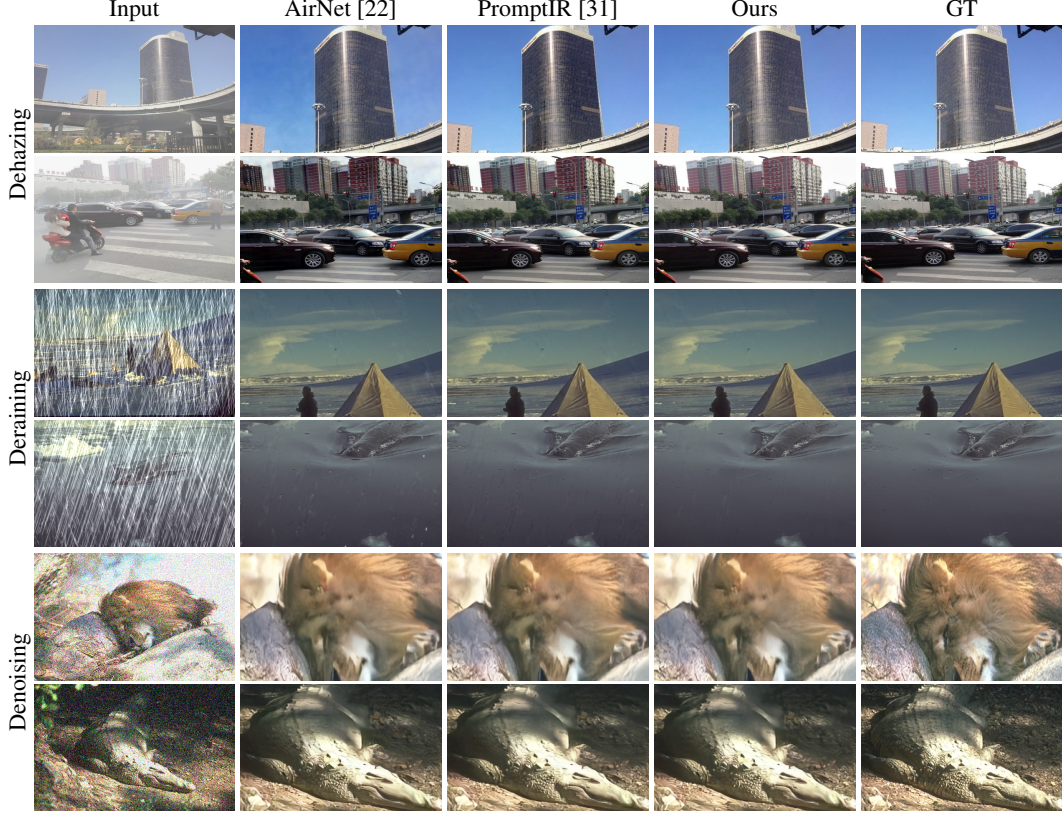


Figure 4: Visual comparison of DaAIR with state-of-the-art methods on challenging cases for the All-in-One setting considering three degradations.

Table 4: *Impact of key components*. PSNR (dB, ↑) and SSIM (↑) metrics are reported on the full RGB images.

Method	\mathcal{E}_D	\mathcal{E}_A	\mathcal{E}_C	\mathcal{L}_{Aux}	PSNR	SSIM
Baseline	-	-	-	-	31.86	.911
(a)	-	✓	✓	-	32.12	.911
(b)	✓	-	✓	✓	32.41	.913
(c)	✓	✓	-	✓	32.44	.913
(d)	✓	✓	✓	-	32.23	.912
DaAIR (ours)	✓	✓	✓	✓	32.51	.913

Table 5: *Complexity Analysis*. GMACS are computed on an input image of size 224×224 using a NVIDIA RTX 4090 GPU.

Method	Memory	Params.	GMACS
AirNet [22]	4829M	8.93M	238G
PromptIR [31]	9830M	35.59M	132G
IDR [54]	4905M	15.34M	98G
DaAIR (ours)	3333M	6.45M	21G

notable performance enhancements. Additionally, for denoising at different noise ratios, our method performs on par with the second-best method, AirNet [22] proving the generality of our approach across multiple degradations.

Visual Results. We show visual results obtained under the three degradation settings in Fig. 4. In certain demanding hazy scenarios, as demonstrated, in Fig. 4, both AirNet [22] and PromptIR [31] reveal constraints in completely eradicating haziness, resulting in noticeable color intensity discrepancies, whereas our approach ensures precise color reconstruction. Furthermore, in challenging rainy scenes, these popular approaches continue to exhibit notable remnants of rain, which our method adeptly eliminates, distinguishing itself from other approaches. Additionally, our method also generates clear and sharp denoised outputs. Coupled with the quantitative comparisons, these findings underscore the effectiveness of our method.

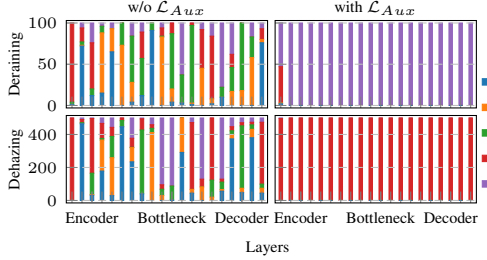


Figure 5: *Routing visualization*. We plot the decisions made by the router \mathcal{R} over the depth of the network.

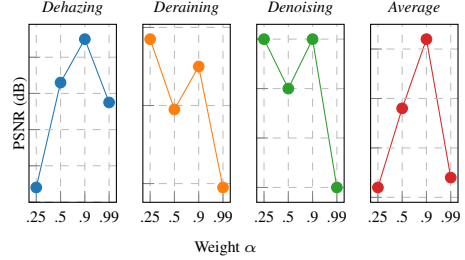


Figure 6: *Impact of α* . We demonstrate the impact of adjusting the influence of encoder parameters on the controller by varying the parameter α .

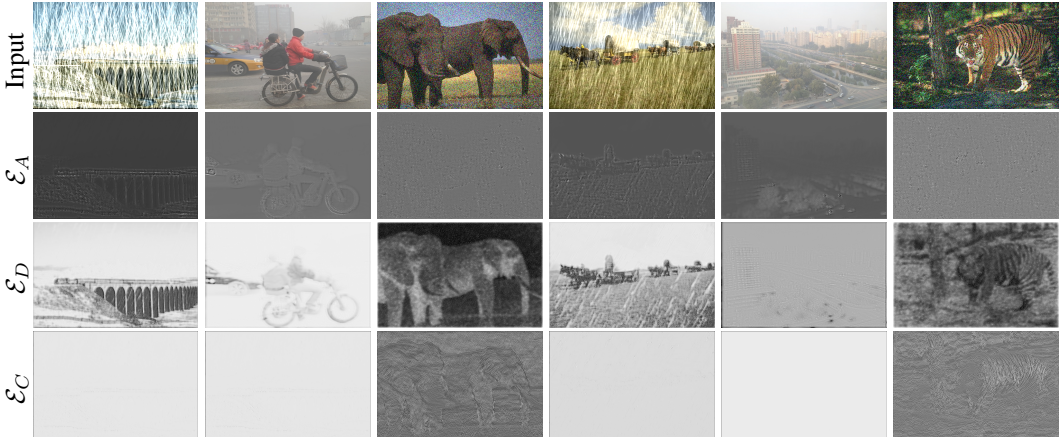


Figure 7: *Feature visualization*. We visualize the features learned by the agnostic expert \mathcal{E}_A and degradation-specific experts \mathcal{E}_D . The controller \mathcal{E}_C adeptly captures degradation-specific patterns, revealing distinct features for various types of corruptions. Zoom in for better view.

4.2 Ablation Studies

We conduct detailed studies on the components within our method. All experiments are conducted in the All-in-One setting with three degradations.

Architecture Contribution. As detailed in Table 4, we assess the efficacy of our proposed key architectural components by contrasting them with a baseline method devoid of our modules. This baseline adopts a scaled-down version of the architecture found in Restormer [53]. Successively integrating the proposed experts and controller into the baseline architecture yields a significant and consistent enhancement. Overall, our framework achieves a notable average improvement of 0.65 dB, attributable to the efficacy of our proposed components and we make the following observations: (i) It is difficult for the model to learn about the degradations without the assistance of the experts, (ii) Incorporation of the controller seems to be beneficial for the overall network learning (w/o controller, the framework’s reconstruction fidelity decreases by an average of 0.28 dB), and (iii) The routing strategy is crucial for the overall performance improvement. The quantitative results in Table 4 (d) and the routing visualization in Fig. 5 highlight the critical role of explicitly correlating routing with the target degradation.

Self-learnable Control. The controller module leverages the accumulated prior knowledge to generate degradation-aware features. It primarily focuses on the most affected regions by updating its parameters via an exponential moving average from the encoder-side agnostic expert which develops an intrinsic understanding of degradations during optimization. We ablate the selection of α , with results visualized in Fig. 6. Our findings reveal that reconstruction performance is sensitive to α , with $\alpha = 0.9$ empirically yielding the best average results and as already discussed above with the

controller, the overall network yields higher performance gain. This demonstrates that leveraging "self-knowledge" significantly enhances the performance of the restorer without incurring additional costs, as agnostic representations are already learned during training. We further visualize and discuss the intricacies learned by the controller in Fig. 7 and Section 5, respectively.

Model efficiency. Table 5 compares memory usage, GMACS, and model parameters, demonstrating our framework's superiority over state-of-the-art All-in-One restorers. By employing a scaled-down Transformer architecture and parameter-efficient experts that process features in a low-rank space, we achieve reductions of 84% in GMACS and 66% in memory consumption compared to PromptIR [31] on an image size 224×224 .

5 Discussion

Our framework incorporates specialized experts at various levels, each dedicated to distinct facets of the restoration problem. These experts either implicitly model degradation specifics, process task-agnostic information or leverage accumulated prior knowledge to control the restoration process. This section aims to elucidate the specific expertise of each component.

Expertized degradation learning. The decision-making process of our degradation-aware routers is illustrated in Fig. 5 (for five degradations). In the absence of the auxiliary degradation classification loss, the selection of experts at each layer does not correspond effectively to the actual type of input degradation. This misalignment results in a more randomized selection, ultimately leading to diminished restoration quality. Although the specific assignment of experts to degradations is arbitrary, maximizing their effectiveness requires a robust router, facilitating the learning of degradation-dependent representations, thereby harnessing the full potential of the parameter-efficient experts. As illustrated in the Fig. 7, the agnostic expert capture general patterns, such as high-frequency details, across different degradations, whereas the specialized experts concentrates strongly on task-related information.

Controller captures degradation characteristics. To underscore the significance of the proposed controller module, we analyze its learned representations, as illustrated in Fig. 7. This analysis vividly demonstrates the controller's adeptness in capturing degradation patterns, elucidating regions afflicted by severe corruption. For instance, in the case of dehazing, where the degradation predominantly impacts the lower frequency spectrum, the controller features manifest a homogeneous distribution. Conversely, while noise presents as stochastic fluctuations in pixel values, impacting higher frequencies, the learned controller features effectively grasps these stochastic variations.

6 Conclusion

This paper introduces DaAIR, an efficient image restoration model that can deal with any type of degradation. Our model sets a new standard in degradation awareness, achieving unparalleled efficiency and fidelity in All-in-One image restoration. In our approach, we intricately design an innovative degradation-aware learner to extract inherent commonalities and capture subtle nuances across various degradations, collaboratively developing a comprehensive degradation-aware representation in the low-rank regime. Specifically, by dynamically allocating the explicit experts to the input degradation, we further enhance the capability of our model. Additionally, we further demonstrate that the degradation-aware representation serves as an effective auxiliary supervisory signal within our method, significantly enhancing the restoration fidelity. Extensive experiments on All-in-One image restoration across diverse degradations reveal that our proposed DaAIR consistently outperforms recent state-of-the-art methods, pushing the boundaries of efficient All-in-One restoration and affirming its practicality.

References

- [1] P. Arbelaez, M. Maire, C. Fowlkes, and J. Malik. Contour detection and hierarchical image segmentation. *IEEE transactions on pattern analysis and machine intelligence*, 33(5):898–916, 2010.

[2] B. Cai, X. Xu, K. Jia, C. Qing, and D. Tao. Dehazenet: An end-to-end system for single image haze removal. *IEEE transactions on image processing*, 25(11):5187–5198, 2016.

[3] L. Chen, X. Chu, X. Zhang, and J. Sun. Simple baselines for image restoration. In *European conference on computer vision*, pages 17–33. Springer, 2022.

[4] Y.-W. Chen and S.-C. Pei. Always clear days: Degradation type and severity aware all-in-one adverse weather removal. *arXiv preprint arXiv:2310.18293*, 2023.

[5] Z. Chen, Y. Zhang, J. Gu, L. Kong, X. Yuan, et al. Cross aggregation transformer for image restoration. *Advances in Neural Information Processing Systems*, 35:25478–25490, 2022.

[6] Z. Chen, Y. Zhang, J. Gu, L. Kong, X. Yang, and F. Yu. Dual aggregation transformer for image super-resolution. In *Proceedings of the IEEE/CVF International Conference on Computer Vision*, 2023.

[7] Y. Cui, S. W. Zamir, S. Khan, A. Knoll, M. Shah, and F. S. Khan. Adair: Adaptive all-in-one image restoration via frequency mining and modulation. 2024.

[8] X. Dang, H. Wang, J. Ren, and L. Chen. An application performance optimization model of mobile augmented reality based on hd restoration. In *2020 Eighth International Conference on Advanced Cloud and Big Data (CBD)*, pages 201–206. IEEE, 2020.

[9] Y. Dong, Y. Liu, H. Zhang, S. Chen, and Y. Qiao. Fd-gan: Generative adversarial networks with fusion-discriminator for single image dehazing. In *Proceedings of the AAAI conference on artificial intelligence (AAAI)*, 2020.

[10] A. Dudhane, O. Thawakar, S. W. Zamir, S. Khan, F. S. Khan, and M.-H. Yang. Dynamic pre-training: Towards efficient and scalable all-in-one image restoration. 2024.

[11] Q. Fan, D. Chen, L. Yuan, G. Hua, N. Yu, and B. Chen. A general decoupled learning framework for parameterized image operators. *IEEE transactions on pattern analysis and machine intelligence*, 43(1):33–47, 2019.

[12] H. Gao, X. Tao, X. Shen, and J. Jia. Dynamic scene deblurring with parameter selective sharing and nested skip connections. In *Proceedings of the IEEE/CVF Conference on Computer Vision and Pattern Recognition (CVPR)*, 2019.

[13] F. Girbacia, S. Butnariu, A. P. Orman, and C. C. Postelnicu. Virtual restoration of deteriorated religious heritage objects using augmented reality technologies. *European Journal of Science and Theology*, 9(2):223–231, 2013.

[14] Q. Hou, C.-Z. Lu, M.-M. Cheng, and J. Feng. Conv2former: A simple transformer-style convnet for visual recognition. *Proceedings of the IEEE Conference on Computer Vision and Pattern Recognition*, 2022.

[15] E. J. Hu, Y. Shen, P. Wallis, Z. Allen-Zhu, Y. Li, S. Wang, L. Wang, and W. Chen. LoRA: Low-rank adaptation of large language models. In *International Conference on Learning Representations*, 2022.

[16] J.-B. Huang, A. Singh, and N. Ahuja. Single image super-resolution from transformed self-exemplars. In *Proceedings of the IEEE Conference on Computer Vision and Pattern Recognition*, pages 5197–5206, 2015.

[17] K. Jiang, Z. Wang, P. Yi, C. Chen, B. Huang, Y. Luo, J. Ma, and J. Jiang. Multi-scale progressive fusion network for single image deraining. In *Proceedings of the IEEE/CVF conference on computer vision and pattern recognition*, pages 8346–8355, 2020.

[18] Y. Jiang, Z. Zhang, T. Xue, and J. Gu. Autodir: Automatic all-in-one image restoration with latent diffusion. *arXiv preprint arXiv:2310.10123*, 2023.

[19] D. P. Kingma and J. Ba. Adam: A method for stochastic optimization, 2017.

[20] J. Lehtinen, J. Munkberg, J. Hasselgren, S. Laine, T. Karras, M. Aittala, and T. Aila. Noise2noise: Learning image restoration without clean data. *arXiv preprint arXiv:1803.04189*, 2018.

[21] B. Li, W. Ren, D. Fu, D. Tao, D. Feng, W. Zeng, and Z. Wang. Benchmarking single-image dehazing and beyond. *IEEE Transactions on Image Processing*, 28(1):492–505, 2018.

[22] B. Li, X. Liu, P. Hu, Z. Wu, J. Lv, and X. Peng. All-In-One Image Restoration for Unknown Corruption. In *Proceedings of the IEEE/CVF Conference on Computer Vision and Pattern Recognition (CVPR)*, 2022.

[23] Z. Li, Y. Lei, C. Ma, J. Zhang, and H. Shan. Prompt-in-prompt learning for universal image restoration. *arXiv preprint arXiv:2312.05038*, 2023.

[24] J. Liang, J. Cao, G. Sun, K. Zhang, L. Van Gool, and R. Timofte. Swinir: Image restoration using swin transformer. In *Proceedings of the IEEE/CVF International Conference on Computer Vision*, 2021.

[25] L. Liu, L. Xie, X. Zhang, S. Yuan, X. Chen, W. Zhou, H. Li, and Q. Tian. Tape: Task-agnostic prior embedding for image restoration. In *Proceedings of the European Conference on Computer Vision (ECCV)*, 2022.

[26] Z. Liu, Y. Lin, Y. Cao, H. Hu, Y. Wei, Z. Zhang, S. Lin, and B. Guo. Swin transformer: Hierarchical vision transformer using shifted windows. In *Proceedings of the IEEE International Conference on Computer Vision*, 2021.

[27] K. Ma, Z. Duanmu, Q. Wu, Z. Wang, H. Yong, H. Li, and L. Zhang. Waterloo exploration database: New challenges for image quality assessment models. *IEEE Transactions on Image Processing*, 26(2):1004–1016, 2016.

[28] D. Martin, C. Fowlkes, D. Tal, and J. Malik. A database of human segmented natural images and its application to evaluating segmentation algorithms and measuring ecological statistics. In *Proceedings of the IEEE International Conference on Computer Vision*, volume 2, pages 416–423. IEEE, 2001.

[29] C. Mou, Q. Wang, and J. Zhang. Deep generalized unfolding networks for image restoration. In *Proceedings of the IEEE/CVF Conference on Computer Vision and Pattern Recognition*, pages 17399–17410, 2022.

[30] S. Nah, T. Hyun Kim, and K. Mu Lee. Deep multi-scale convolutional neural network for dynamic scene deblurring. In *Proceedings of the IEEE conference on computer vision and pattern recognition*, pages 3883–3891, 2017.

[31] V. Potlapalli, S. W. Zamir, S. Khan, and F. Khan. Promptir: Prompting for all-in-one image restoration. In *Thirty-seventh Conference on Neural Information Processing Systems (NeurIPS)*, 2023.

[32] K. Purohit, M. Suin, A. Rajagopalan, and V. N. Boddeti. Spatially-adaptive image restoration using distortion-guided networks. In *Proceedings of the IEEE/CVF international conference on computer vision*, pages 2309–2319, 2021.

[33] Y. Qu, Y. Chen, J. Huang, and Y. Xie. Enhanced pix2pix dehazing network. In *Proceedings of the IEEE/CVF conference on computer vision and pattern recognition*, pages 8160–8168, 2019.

[34] D. Ren, W. Zuo, Q. Hu, P. Zhu, and D. Meng. Progressive image deraining networks: A better and simpler baseline. In *Proceedings of the IEEE/CVF conference on computer vision and pattern recognition*, pages 3937–3946, 2019.

[35] W. Ren, L. Ma, J. Zhang, J. Pan, X. Cao, W. Liu, and M.-H. Yang. Gated fusion network for single image dehazing. In *Proceedings of the IEEE conference on computer vision and pattern recognition*, pages 3253–3261, 2018.

[36] W. Ren, J. Pan, H. Zhang, X. Cao, and M.-H. Yang. Single image dehazing via multi-scale convolutional neural networks with holistic edges. *International Journal of Computer Vision*, 128:240–259, 2020.

[37] C. Riquelme, J. Puigcerver, B. Mustafa, M. Neumann, R. Jenatton, A. Susano Pinto, D. Keysers, and N. Houlsby. Scaling vision with sparse mixture of experts. In *Advances in Neural Information Processing Systems*, 2021.

[38] O. Ronneberger, P. Fischer, and T. Brox. U-Net: Convolutional networks for biomedical image segmentation. In *Proceedings of International Conference on Medical Image Computing and Computer-Assisted Intervention*, pages 234–241. Springer, 2015.

[39] G. Saggio, D. Borra, et al. Augmented reality for restoration/reconstruction of artefacts with artistic or historical value. In *Augmented reality: some emerging application areas*, pages 59–86. InTech Publications, 2011.

[40] N. Shazeer, A. Mirhoseini, K. Maziarz, A. Davis, Q. Le, G. Hinton, and J. Dean. Outrageously large neural networks: The sparsely-gated mixture-of-experts layer. *arXiv preprint arXiv:1701.06538*, 2017.

[41] Y. Tai, J. Yang, X. Liu, and C. Xu. Memnet: A persistent memory network for image restoration. In *Proceedings of the IEEE international conference on computer vision*, pages 4539–4547, 2017.

[42] C. Tian, Y. Xu, and W. Zuo. Image denoising using deep cnn with batch renormalization. *Neural Networks*, 2020.

[43] J. M. J. Valanarasu, R. Yasarla, and V. M. Patel. Transweather: Transformer-based restoration of images degraded by adverse weather conditions. In *Proceedings of the IEEE/CVF Conference on Computer Vision and Pattern Recognition (CVPR)*, 2022.

[44] C. Wang, J. Pan, W. Wang, J. Dong, M. Wang, Y. Ju, and J. Chen. Promptrestorer: A prompting image restoration method with degradation perception. In *Thirty-seventh Conference on Neural Information Processing Systems*, 2023. URL <https://openreview.net/forum?id=nIaNgQvsV>.

[45] Z. Wang, X. Cun, J. Bao, W. Zhou, J. Liu, and H. Li. Uformer: A general u-shaped transformer for image restoration. In *Proceedings of the IEEE/CVF Conference on Computer Vision and Pattern Recognition (CVPR)*, pages 17683–17693, June 2022.

[46] C. Wei, W. Wang, W. Yang, and J. Liu. Deep retinex decomposition for low-light enhancement. *arXiv preprint arXiv:1808.04560*, 2018.

[47] H. Wu, Y. Qu, S. Lin, J. Zhou, R. Qiao, Z. Zhang, Y. Xie, and L. Ma. Contrastive learning for compact single image dehazing. In *Proceedings of the IEEE/CVF conference on computer vision and pattern recognition*, pages 10551–10560, 2021.

[48] F. Yang, H. Yang, J. Fu, H. Lu, and B. Guo. Learning texture transformer network for image super-resolution. In *Proceedings of the IEEE/CVF conference on computer vision and pattern recognition*, pages 5791–5800, 2020.

[49] R. Yasarla and V. M. Patel. Uncertainty guided multi-scale residual learning-using a cycle spinning cnn for single image de-raining. In *Proceedings of the IEEE/CVF conference on computer vision and pattern recognition*, pages 8405–8414, 2019.

[50] S. W. Zamir, A. Arora, S. Khan, M. Hayat, F. S. Khan, M.-H. Yang, and L. Shao. Cycleisp: Real image restoration via improved data synthesis. In *Proceedings of the IEEE/CVF conference on computer vision and pattern recognition*, pages 2696–2705, 2020.

[51] S. W. Zamir, A. Arora, S. Khan, M. Hayat, F. S. Khan, M.-H. Yang, and L. Shao. Learning enriched features for real image restoration and enhancement. In *Computer Vision–ECCV 2020: 16th European Conference, Glasgow, UK, August 23–28, 2020, Proceedings, Part XXV 16*, pages 492–511. Springer, 2020.

[52] S. W. Zamir, A. Arora, S. Khan, M. Hayat, F. S. Khan, M.-H. Yang, and L. Shao. Multi-stage progressive image restoration. In *Proceedings of the IEEE/CVF Conference on Computer Vision and Pattern Recognition (CVPR)*, 2021.

[53] S. W. Zamir, A. Arora, S. Khan, M. Hayat, F. S. Khan, and M.-H. Yang. Restormer: Efficient transformer for high-resolution image restoration. In *Proceedings of the IEEE/CVF Conference on Computer Vision and Pattern Recognition (CVPR)*, 2022.

- [54] J. Zhang, J. Huang, M. Yao, Z. Yang, H. Yu, M. Zhou, and F. Zhao. Ingredient-oriented multi-degradation learning for image restoration. In *Proceedings of the IEEE/CVF Conference on Computer Vision and Pattern Recognition (CVPR)*, 2023.
- [55] K. Zhang, W. Zuo, S. Gu, and L. Zhang. Learning deep cnn denoiser prior for image restoration. In *Proceedings of the IEEE conference on computer vision and pattern recognition*, pages 3929–3938, 2017.
- [56] K. Zhang, W. Zuo, and L. Zhang. Ffdnet: Toward a fast and flexible solution for cnn-based image denoising. *IEEE Transactions on Image Processing*, 27(9):4608–4622, 2018.
- [57] Y. Zhang, Y. Tian, Y. Kong, B. Zhong, and Y. Fu. Residual dense network for image super-resolution. In *Proceedings of the IEEE Conference on Computer Vision and Pattern Recognition*, 2018.
- [58] Y. Zhang, K. Li, K. Li, B. Zhong, and Y. Fu. Residual non-local attention networks for image restoration. *arXiv preprint arXiv:1903.10082*, 2019.
- [59] H. Zhao, Y. Gou, B. Li, D. Peng, J. Lv, and X. Peng. Comprehensive and delicate: An efficient transformer for image restoration. In *Proceedings of the IEEE/CVF conference on computer vision and pattern recognition*, pages 14122–14132, 2023.

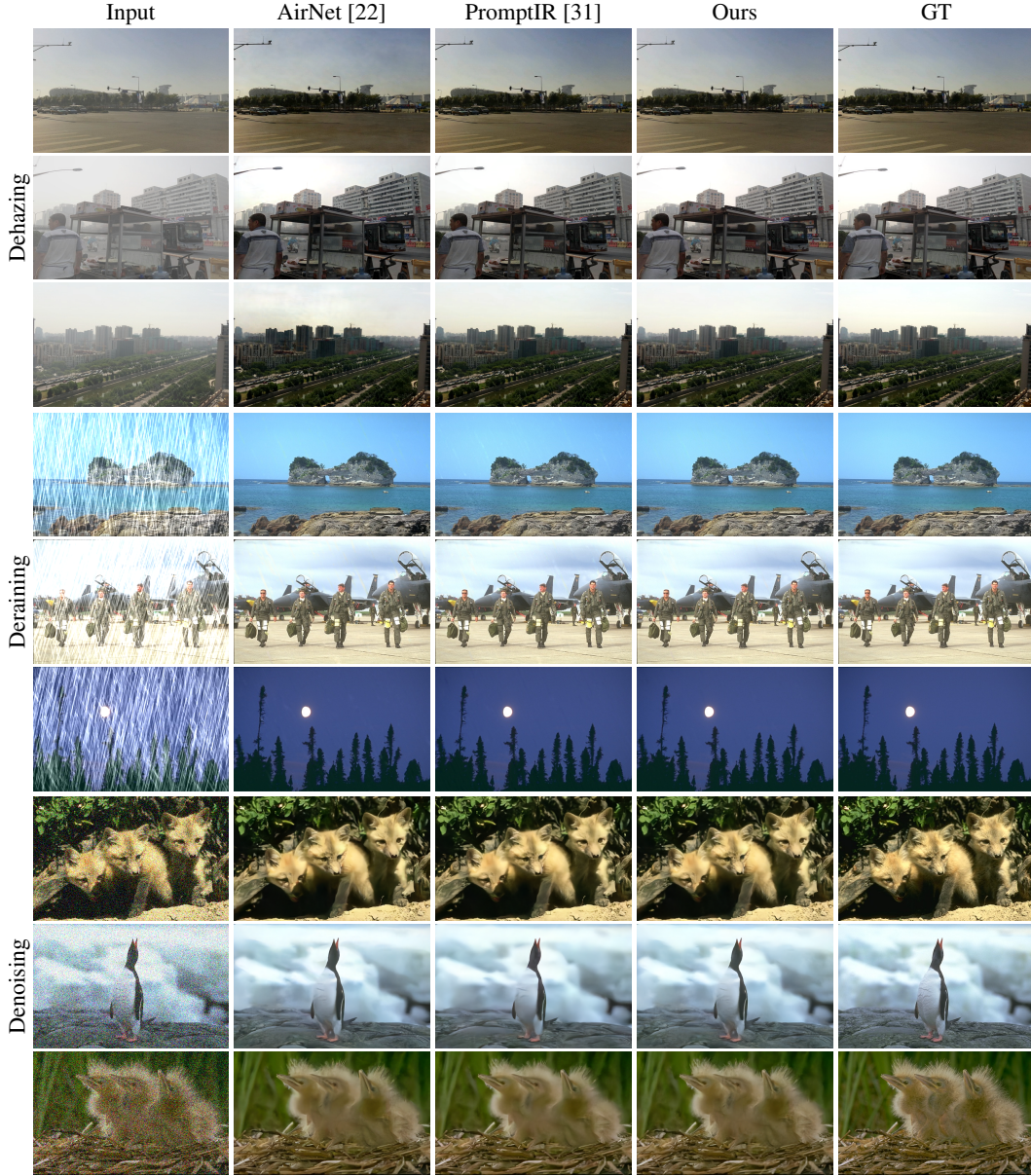


Figure 8: Visual comparison of DaAIR with state-of-the-art methods on challenging cases for the All-in-One setting considering three degradations.

A Further Implementation Details

Across all experiments, we maintain a consistent random seed to ensure reproducibility. Our implementation was built upon the publicly available PyTorch-based *PromptIR* codebase, leveraging it for architecture development and training. Additionally, we employed the *fvcore* Python package to compute GMACS and parameter counts.

Baseline for architecture ablation. In this section, we elaborate on the baseline method utilized for the ablation study presented in Table 4. Our model is constructed upon the Restormer architecture [53], akin to previous All-in-One models [31, 10]. However, we implement modifications by reducing the number of blocks within each level of the encoder and decoder, while initializing the input embedding size to 32, progressively doubling it in subsequent levels. Furthermore, within our final model, we



Figure 9: *More feature visualization.* We visualize the features learned by the agnostic expert \mathcal{E}_A , degradation-specific experts \mathcal{E}_D and the controller \mathcal{E}_C . Zoom in for better view.

replace the channel-wise self-attention layer on the decoder side of the UNet [38] architecture by cross-attention between controller features \mathbf{x}_C and the modulated features $\hat{\mathbf{x}}$ stemming from DaLe.

B Future Work and Limitations

The proposed DaAIR framework models degradation dependencies by allocating dedicated modeling capacity to individual tasks. Enhancing this framework with external inductive biases, such as edge information or frequency-related constraints, could improve the simultaneous handling of multiple degradation types, rather than relying solely on implicit degradation learning. Moreover, while this work utilizes synthetically degraded images, which have a significant domain gap from realistic scenarios, applying DaAIR to more complex, realistic degradation settings represents a promising direction for future research.

C Visual Results

We provide additional visual results in Fig. 8 and feature visualizations in Fig. 9 to further underscore the strong restoration fidelity of our framework and the expressiveness of the learned features. These visualizations highlight the effectiveness of our approach in capturing intricate details and improving image quality across various degradation scenarios.